Int. J. Pres. Ves. & Piping **13** (1983) 107–125

Failure Assessment Diagrams and *J* Estimates: A Comparison for Ferritic and Austenitic Steels

I. Milne

Central Electricity Generating Board,
Technical Planning and Research Division,
Central Electricity Research Laboratories,
Kelvin Avenue, Leatherhead, Surrey, Great Britain

(Received: 28 July, 1982)

ABSTRACT

Comparisons are made between the R6 assessment procedures and a J *estimation procedure for a number of specimen geometries made of A533B steel and an austenitic steel. The two procedures differ in three important respects:*

(*i*) *The R6 procedures make explicit use of the plastic limit load of a structure while, for the* J *estimate, this can only be inferred from the load at which* J *increases rapidly.*

(*ii*) *The R6 procedures use a flow stress, generally equal to the arithmetic mean of the yield and ultimate tensile stress, to define this plastic limit load while the* J *estimate attempts to allow for strain hardening using the Ramberg–Osgood law.*

(*iii*) *The R6 procedures interpolate between the linear elastic and fully plastic limits using a modification of the strip yielding model while the* J *estimates use a first order plasticity correction.*

Despite these differences, it is shown that for most structures built of A533B steel the R6 procedures can be expected to give results comparable to the J *estimates. However, for structures built of austenitic steel there is a need to make an explicit allowance for strain hardening.*

The accuracy of the J *estimates depends upon how closely the Ramberg–Osgood law fits the material's true stress–true strain curve. This, in turn, depends upon the strain hardening capacity of the material.*

Int. J. Pres. Ves. & Piping 0308-0161/83/$03·00

The fit is only satisfactory when the strain hardening capacity is low. Thus the J estimates, although of proven reliability for some geometries of A533B, can still be seriously in error for austenitic steels. Even for A535B steels the nature of the Ramberg–Osgood law produces a tendency to overestimate plastic limit loads.

A strain hardening form of the R6 procedures is developed which avoids these problems. It is based upon the ratio of the ultimate to yield stresses obtained from the engineering stress–strain curve. It is demonstrated that although this form of the R6 procedures is in good agreement with the results of test data from compact specimens of austenitic steels, the modification will have an insignificant effect on the results obtained for ferritic steels. It can also be presented in a diagrammatic form which is particularly suitable for code applications.

INTRODUCTION

Various comparisons have been made between elastic–plastic fracture mechanics solutions obtained from J integral studies and from the CEGB procedure, R6.[1–3] Most of these comparisons have concluded that the R6 procedures are satisfactory and, in general, pessimistic, for most geometries and materials. However, some reservations have been expressed about materials with a high capacity for strain hardening, e.g. austenitic alloys, and about a possible geometry dependence of the assessment line.

The R6 procedures differ from a J analysis in three important respects:

(1) The explicit use of a plastic limit load.
(2) The use of a flow stress criterion to define this limit load rather than a strain hardening law.
(3) The concept that for all practical purposes the elastic–plastic effects for all geometries can be represented by the infinite plate solution of the strip yielding model (the log sec equation).

These three features of the R6 procedures have been fully vindicated by a considerable amount of experimental data.[4] Nevertheless, there remains some doubt as to why the simplistic approach of R6 works, and hence whether and under what conditions more elaborate procedures are necessary. This paper compares J solutions for a number of geometries and two different materials with the R6 procedures. It will be demonstrated that for ferritic steels the R6 procedures are generally

satisfactory. For austenitic steels, the procedures need to be modified to take account of the high strain hardening capacity of these materials and a suitable modification is proposed and validated against load-displacement data obtained from compact tension test pieces.

BASIS OF COMPARISON

The scheme developed by Kumar *et al.*[3] will be used as the basic means for evaluating J for the comparisons. In this scheme J is evaluated from two terms as:

$$J = J_{FP} + J_{FOP} \tag{1}$$

Here J_{FP} is a fully plastic solution for J with the general form:

$$J_{FP} = \alpha\varepsilon_o\sigma_o(w-a)h_1(n, a/W, P_o)(P/P_o)^{n+1} \tag{2}$$

where σ_o is the uniaxial yield stress at the strain, ε_o; α and n are obtained from fitting the Ramberg–Osgood equation to the stress–strain curve; P is the applied load; P_o a reference load based upon σ_o; h is a function determined by fitting J_{FP} to a fully plastic finite element J solution for the geometry in question and W and a are the structure's width and crack depth, respectively. Values for h_1 have been tabulated by Kumar *et al.*,[3] as a function of n for a number of geometries.

J_{FOP} is a linear elastic solution for J corrected for small-scale plasticity using a modification of Irwin's first order plastic zone correction and has the form:

$$J_{FOP} = \frac{K^2(a_e)}{E'} \tag{3}$$

where E' is $E/(1-\nu^2)$, for plane strain and E for plane stress, E being Young's modulus and ν being Poisson's ratio; $K(a_e)$ is the elastic stress intensity factor and $a_e = a + \phi r_y$ where

$$\phi = 1/1 + (P/P_o)^2 \qquad \text{and} \qquad r_y = \frac{1}{B\pi}\frac{n-1}{n+1}(K(a)/\sigma_o)^2$$

β is 6 for plane strain and 2 for plane stress.

In so far as J_{FP} is a measure of J under fully plastic conditions and J_{FOP} interpolates between this and the linear elastic limit, the Kumar *et al.*[3]scheme bears strong similarities to the R6 procedures. It differs in that

it has been evolved as a parametric fit to finite element solutions for J, so that the plastic collapse limit is not included explicitly. The plastic limit is normally inferred from the load at which J becomes infinite.

The equivalence between the R6 procedures and a J analysis has been demonstrated by Chell[1] and Chell and Milne.[5] The equation for the R6 assessment line is:

$$K_r = S_r \left\{ \frac{8}{\pi^2} \ln \sec \left(\frac{\pi}{2} S_r \right) \right\}^{-1/2} \tag{4}$$

where K_r can be defined as $\sqrt{G/J}$, G being the elastic strain energy release rate and $S_r = P/P_1$. S_r can equally well be defined in terms of stresses, but defining it in loads demonstrates that it must be expressed in terms of the load which the uncracked ligament can support and that this must take into account the strain hardening properties of the material. Experimental plastic collapse data will define P_1 explicitly and automatically include any strain hardening effects. The experimental data lead to an empirical formula for the collapse stress, $\sigma_1(a/W)$, which, in general, can be expressed as:

$$\sigma_1 = \sigma_f f(a/W)$$

where σ_f is a flow stress which is generally equated to $\frac{1}{2}(\sigma_y + \sigma_u)$, i.e. the arithmetic mean of the uniaxial yield and ultimate tensile stress.

STRESS–STRAIN DATA

Two stress–strain curves were used for the comparison, one for the ferritic pressure vessel steel A533B published by Issler *et al.*,[6] the other for the austenitic stainless steel used in the ASTM E24 predictive 'Round Robin' exercise.[7] True stress–true strain plots of these data are presented in Figs 1(a) and 1(b). The Ramberg–Osgood strain hardening law:

$$\frac{\varepsilon}{\varepsilon_o} = \frac{\sigma}{\sigma_o} + \alpha \left(\frac{\sigma}{\sigma_o} \right)^n \tag{5}$$

was fitted to these true stress–true strain curves with the aid of a log–log plot to give the parameters listed on the figures. The stress–strain curves predicted from eqn. (5) are compared with the measured curves in Figs. 1(a) and (b).

The A533B steel had a modest capacity for strain hardening, and a

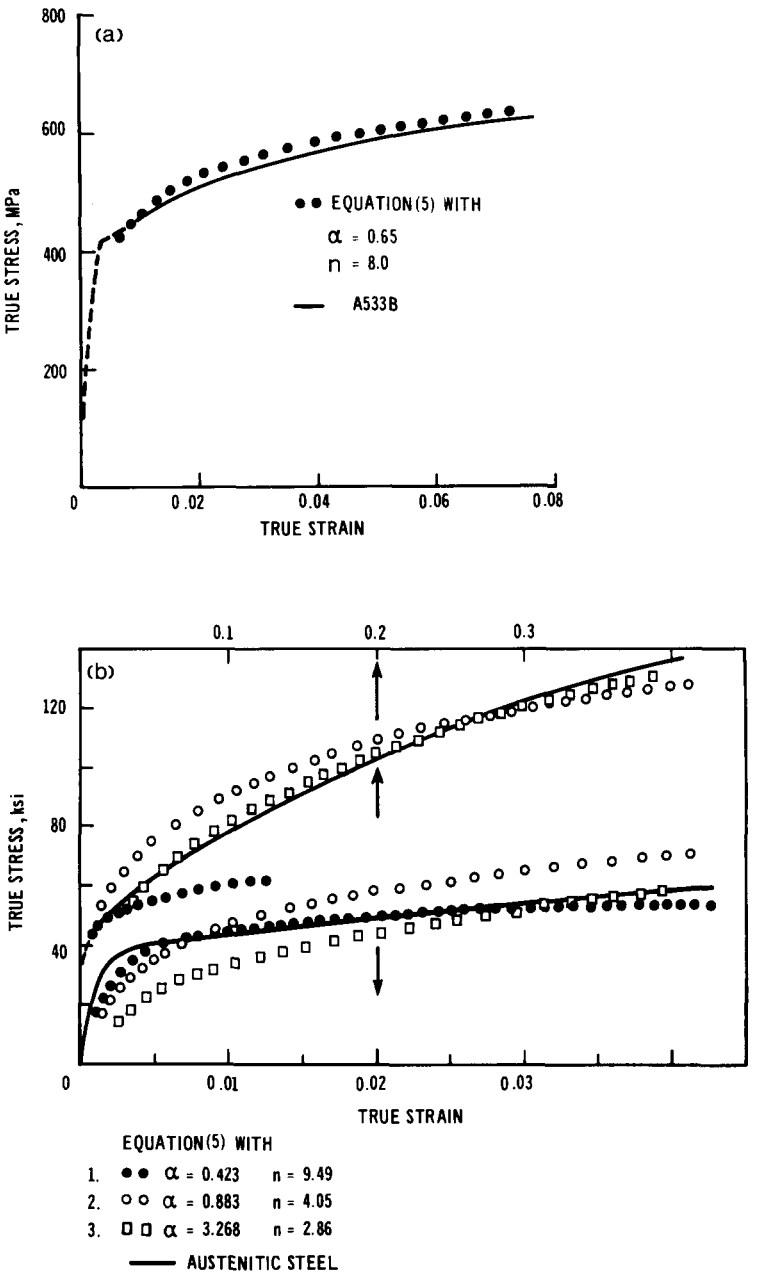

Fig. 1. (a) True stress–true strain curve for A533B steel (After Issler *et al.*[6]). (b) True stress–true strain curve for γ steel (After Newman[7]).

reasonable fit was obtained between eqn. (6) and the whole of the experimental data with $\alpha = 0{\cdot}65$ and $n = 8$. On the other hand, the austenitic steel had a large capacity for strain hardening so that no general satisfactory fit could be obtained between eqn. (5) and these data. Three combinations of α and n were therefore obtained; the first to give a good fit at low strains, the second to give a good fit at high strains and the third to give as good a fit as possible over the total strain range. (See Fig. 1b.) It has previously been observed[6] that different values of α and n obtained from the same stress–strain curve can produce significantly different J estimates.

J ESTIMATES AND COMPARISON WITH R6

Estimates of J/G for the three-point bend specimen shown have been plotted as a function of applied load in Figs 2(a) and (b) for the four stress–strain relationships obtained. The applied load, P, has been

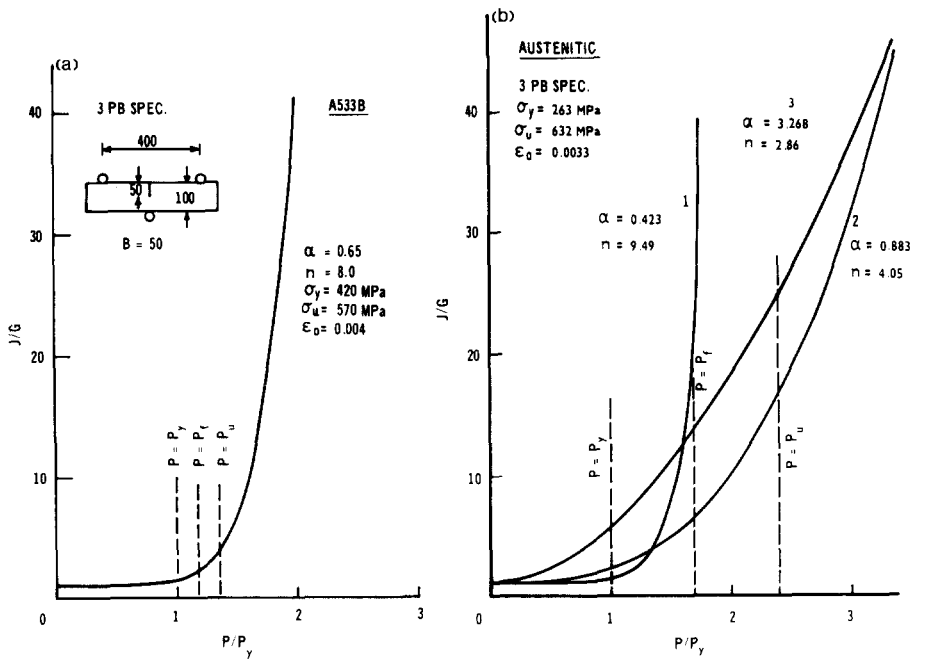

Fig. 2. (a) Plot of J/G versus P/P_y for a three-point bend specimen of A533B. (b) Plot of J/G versus P/P_y for the three-point bending specimen of Fig. 2(a) mode of γ steel.

normalised by the yield limit load, P_y, obtained from the Green–Hundy relationship:

$$P_y = 1{\cdot}456\sigma_y(w-a)^2B/S$$

where σ_y is the yield stress* and S is the span. Three load levels have been indicated on the abscissa of each Figure: when $P = P_y$, when $P = P_u$ and when $P = P_f$. P_u and P_f were evaluated from the Green–Hundy equation by replacing σ_y by ultimate and flow stresses of the material. The flow stress was taken as $\frac{1}{2}(\sigma_y + \sigma_u)$.

Two important points emerge from these Figures: (i) for the austenitic material, the J solutions are widely different, depending upon the α and n values chosen, as was previously observed by Issler *et al.*,[6] (ii) in all but one case the plastic limit loads are badly defined and/or severely overestimated.

These results are compared with the R6 assessment line in Figs 3(a) and (b). It is apparent that the J solution for A533B, Fig. 3(a), is adequately represented by the R6 diagram, using σ_f as the collapse criterion, while none of the J solutions for the austenitic steel can be represented by this diagram, Fig. 3(b).

The three-point bend specimen was chosen for this example because the conditions for plastic collapse of this specimen are well understood and have been validated experimentally on many occasions using ferritic steels. The comparative behaviour shown in Figs 1, 2 and 3 is, however, typical of all geometries analysed to date, including compact tension, double edged cracked tension and centre crack tension test pieces. This behaviour can be summarised as follows.

(1) For ferritic materials (or materials whose stress–strain curves can be closely represented by eqn. (5) at all levels of strain) the R6 assessment line gives similar results to a J-analysis for all values of $J \lesssim 4G$, regardless of geometry.
(2) For austenitic materials (or materials with a large capacity for strain hardening) the R6 assessment line does not approximate to any of the J solutions. In this instance the effects of strain hardening cannot be represented by a flow stress.

* Kumar *et al.*[3] define a reference load, P_o, relative to σ_o, where σ_o is the yield stress for the material. In defining P_y as the yield load the term σ_y will be used to define the yield stress. Thus, in the text, σ_y and σ_o can be interchanged, but P_y and P_o cannot.

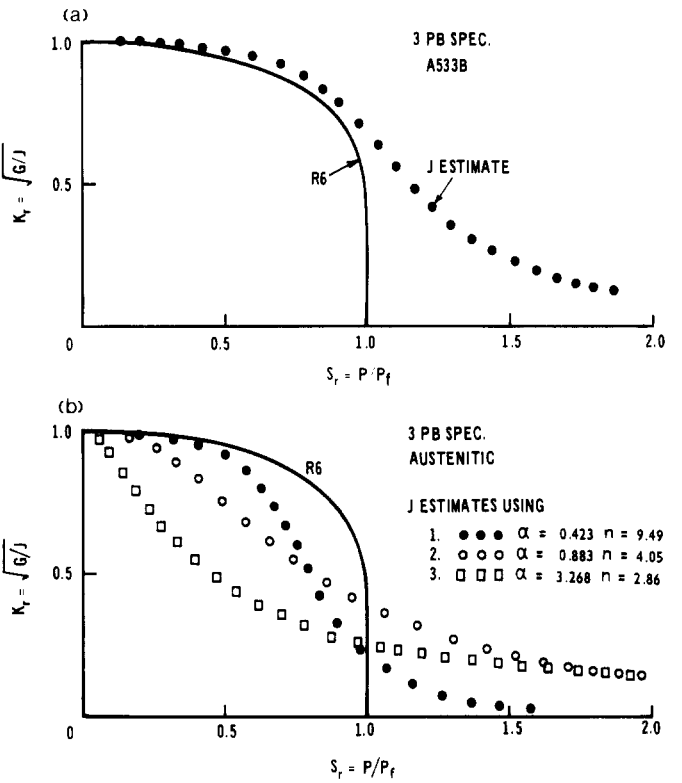

Fig. 3. (a) Comparison of J estimation for three-point bending specimen of A533B with R6 assessment line. (b) Comparison of J estimates for three-point bending specimen of γ steel characterised as indicated, and the R6 assessment line.

(3) The flow properties of austenitic materials (of materials with a large capacity for strain hardening) cannot be represented satisfactorily by eqn. (5).

(4) In general, the J solutions derived using the constants of eqn. (5) provide an ill-defined overestimate of known plastic collapse solutions.

AN R6 STRAIN HARDENING DIAGRAM

The strain hardening assessment lines proposed by Bloom[2] are based upon an inversion of the J solutions of Kumar *et al.*[3] plotted as a function of S_r, with the collapse limit expressed in terms of P_o. While this form of assessment line has the advantage of an inbuilt allowance for

strain hardening, it suffers the disadvantages listed above; namely α and n need to be known and need to be relevant, and the plastic collapse limit is generally badly defined. In addition, to be rigorous, a new assessment line has to be developed for each combination of α and n, and for each geometry. The geometry dependence is caused partly by the dependence of J_{FP} on α and n, and partly through a loose definition for P_o. If S_r is defined in terms of P_y rather than P_o, this geometry dependence largely disappears. This feature is, however, contingent upon eqn. (5) being a good representation of the material's true stress–true strain curve. If this is not so, a strong geometry dependence will still appear in the strain hardening assessment lines. Such a geometry dependence is an artefact of eqn. (5), however, and is not observed in practice (see the next two sections).

To avoid these problems and to provide a more rational basis for performing an engineering assessment which takes explicit account of the strain hardening properties of a material, the following modification to the equation for the R6 assessment line is proposed:

$$S_r = \frac{\sigma}{\sigma_y} + (1 - K_r^{1/2})\left(\frac{\sigma_u}{\sigma_y} - 1\right) \tag{6(a)}$$

$$K_r = \frac{\sigma/\sigma_y}{\sqrt{\frac{8}{\pi^2} \ln \sec\left(\frac{\pi}{2}\frac{\sigma}{\sigma_y}\right)}} \tag{6(b)}$$

where σ is the applied stress, σ_y is the yield stress and σ_u is the ultimate tensile stress obtained from an engineering stress–strain curve for the material. This modification retains the log sec form of the strip yield model through eqn. (6(b)), but the plasticity correction is interpolated between σ_y and σ_u via the last term in eqn. (6(a)). This term was chosen so that, at high values of K_r (i.e. at $J/G < 4$), plasticity effects are determined by σ_y; at moderate levels of $K_r (4 < J/G < 16)$ plasticity effects are determined by σ_f; at low levels of K_r plasticity effects are determined by σ_u. The analysis is performed as conventionally required of R6, with the co-ordinates of the assessment point defined in general as:

$$S_r = \frac{\sigma}{\sigma_y f(c/w)} = \frac{P}{P_y} \tag{7(a)}$$

$$K_r = \sqrt{\frac{G}{J}} \quad \text{or} \quad \frac{K_1}{K_\Omega} \tag{7(b)}$$

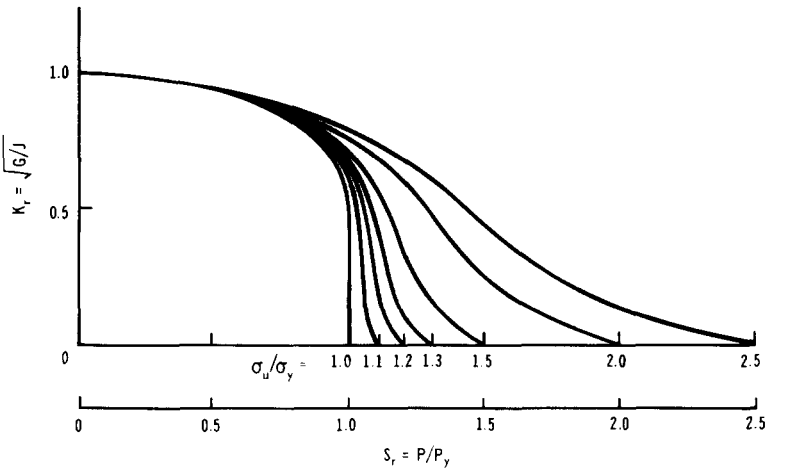

Fig. 4. The R6 assessment line modified for strain hardening (eqn. (6)).

where $\sigma_y f(c/w)$ is the plastic limit stress defined by σ_y, and $J_R = E' K_\Omega$ is the material toughness property.

A series of curves has been generated for different ratios of σ_u/σ_y and is plotted in Fig. 4. The similarity between this type of curve and the curves developed from the J estimates (Fig. 3) is apparent, especially for $K_r \lesssim 0{\cdot}25$ ($J/G \gtrsim 16$). Outside this range, these curves intersect the abscissa at $S_r = \sigma_u/\sigma_y$, and so avoid the problem of overpredicting the load capacity of the structure at high levels of J/G.

VALIDATION OF THE R6 STRAIN HARDENING DIAGRAM

In Figure 5 the assessment line derived from eqn. (2) is compared with the conventional R6 assessment line renormalised to $S_r = P/P_y$, for the A533B steel. Also plotted on this diagram are assessment lines derived from J for a three-point bend geometry, a centre cracked panel and a double edged cracked tensile piece. The overestimation of the plastic collapse loads from the J estimates is apparent for $K_r \lesssim 0{\cdot}5$ for the three-point bend double edged notched specimen and for $K_r < 0{\cdot}25$ for the centre cracked panel. However, apart from this, the correspondence between any of these assessment lines is very good, and well within the accuracy expected of any analysis. It is clear that eqn. (6) provides a good approximation to the J solutions obtained for these geometries and

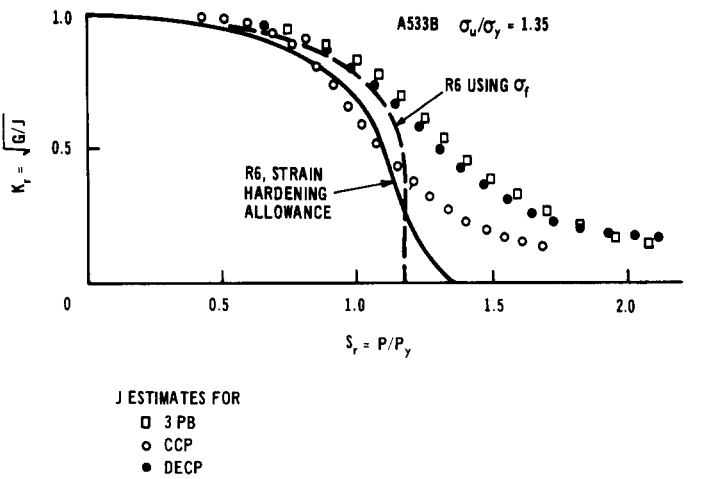

Fig. 5. Comparison of eqn. (6) with J estimates for three geometries of A533B.

A533B steel. Moreover, in the elastic–plastic regions, i.e. at $K_r \gtrsim 0{\cdot}5$, these solutions never deviate more than a few per cent from the original R6 assessment line. Since the validity of this line has been demonstrated experimentally for a large number of additional geometries, including a cracked nozzle,[4] it is reasonable to conclude that eqn. (6) can be used for most geometries of practical interest made of ferritic steel.

For austenitics the situation is rather more difficult to prove, mainly because of the difficulty in defining α and n (eqn. (5)) and the sensitivity of the J solutions to these parameters. Furthermore, experimental data suitable for validation purposes is not readily available. In general the toughness of austenitic steels is so high that, for most specimens and structures which have been tested to date, crack growth does not begin until the maximum load has been reached. The maximum load appears to be adequately represented by collapse criteria defined by the flow stress, $\frac{1}{2}(\sigma_y + \sigma_u)$, Kanninen *et al.*,[8] but this observation is not, on its own, sufficient for validation.

In the ASTM E24 'Round Robin' exercise,[7] values of load and load line displacement were tabulated for three compact tension specimens of the austenitic steel characterised above; J resistance data were also presented but these appear to be unreliable, being linear with crack growth and passing through the origin. Crack sizes (and hence growth) were also tabulated as a function of load, as implied by unloading compliance measurements. From these tabulations, load–load line displacement

curves were generated, an example of which is shown in Fig. 6. The accompanying load–crack size plot shows that the crack did not grow until the maximum load had been reached. This is testimony to the unreliability of the J resistance curves, since, at this point, J was very large.

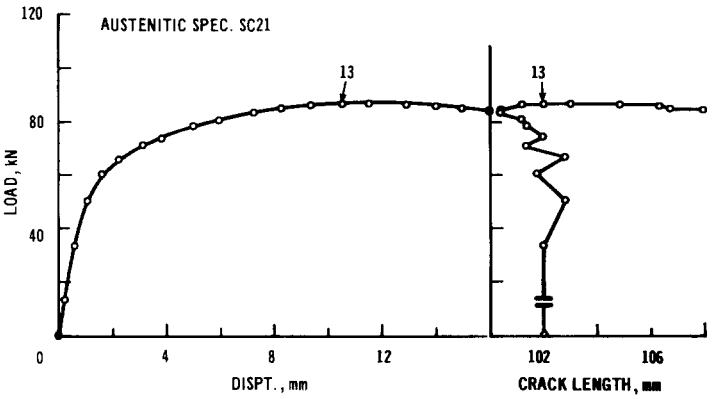

Fig. 6. Load–displacement and crack growth curves for γ steel compact tension specimen, after Newman.[7]

The ratio $K_r = \sqrt{G/J}$ was calculated from these load displacement curves as a function of applied load, P. S_r was also calculated as the ratio of P/P_y where P_y is the load to yield the specimen given by $m\sigma_y BW$, where $m^2 + 2m(1 + a/W) = (1 - a/W)^2$ (Haigh and Richards[9]). The resultant co-ordinates, $S_r K_r$, are shown plotted on Fig. 7 and compared with the assessment line defined by eqn. (6) and the lines produced by the J solutions using the three combinations of α and n obtained from Fig. 1(b). The experimental results are well represented by the line defined in eqn. (6). They also lie close to the J solution labelled 1, obtained using $\alpha = 0{\cdot}423$ and $n = 9{\cdot}49$, but only for $S_r < 1$. This J solution was obtained from the stress–strain relationship which provided a good fit to the experimental stress–strain curve at low strains only. The other J solutions were obviously totally inadequate in falling well below the data at levels of S_r below $\sim 1{\cdot}5$ to $1{\cdot}6$.

It should be emphasised that the data plotted in Fig. 7 are mainly pre-maximum load data and that no crack growth had occurred prior to the maximum load in any of the cases. All the solutions tend to converge at the point of maximum load; in this case where $S_r \simeq 1{\cdot}6$ to $1{\cdot}8$. A value of

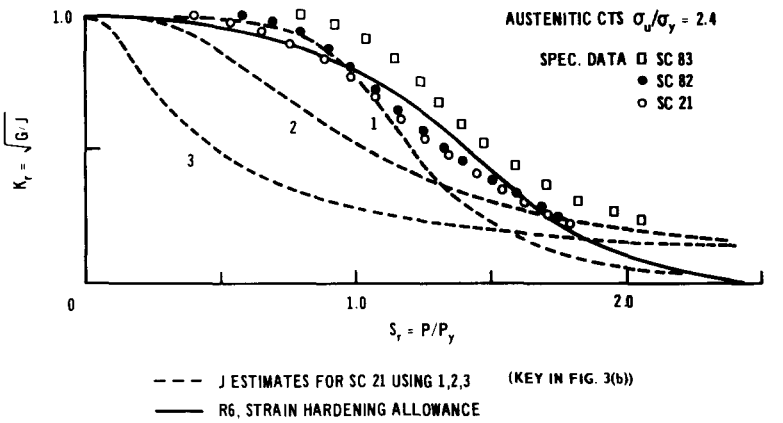

Fig. 7. Comparison of eqn. (6), J estimates and experimental data for compact tension specimens of γ steel.

$S_r = 1{\cdot}7$ would be derived for the maximum load from the flow stress definition of S_r, with $\sigma_f = \frac{1}{2}(\sigma_y + \sigma_u)$. Bloom[2] also derived J solutions for these geometries using a value of $\alpha = 3{\cdot}324$ and $n = 3{\cdot}816$. When plotted against P/P_y as defined above, these solutions lie a little below the J solutions (2) for $\alpha = 0{\cdot}883$ and $n = 4{\cdot}05$ (Fig. 7) and converge to both the experimental data and the other J solutions again at $1{\cdot}6 < S_r < 1{\cdot}8$. Since, in this regime, all the solutions will give results to within a few per cent of each other, good predictions of maximum loads and post-maximum load behaviour will give unreliable indications of the validity of any of these J solutions. It is clearly necessary to plot out a full assessment line as a function of load, and test it in the region where plasticity effects are small, as well as in the fully plastic region. When this is done, it is quite clear that eqn. (6) gives a better fit to the experimental data than any of the other solutions.

THE RAMBERG–OSGOOD LAW

The problem with the J solutions for the austenitic materials lies in the nature of the Ramberg–Osgood law. This law can be used to provide a reasonable representation of the true stress–true strain curves of materials with a low capacity for strain hardening, such as moderate to high strength ferritic steels. However, as the strain hardening capacity

increases, it becomes increasingly more difficult to fit the Ramberg–Osgood law to the stress–strain curve of the material.

For example, at $\sigma/\sigma_o = 1$, eqn. (5) predicts that $\varepsilon/\varepsilon_o = 1 + \alpha$. A high value of α therefore predicts excessive non-linearity at low strains. A good fit at high strains to the austenitic data in Fig. 1(b) was provided by a low value of n and a high value of α, but this produced a poor fit at low strains. A good fit at low strains can result only from low values of α, coupled with high values of n. This tends to flatten the curve at high strains.

Although this feature of the Ramberg–Osgood law is apparent in Fig. 1(b) its effects are more easily discussed from the viewpoint of Fig. 8. Here, eqn. (5) has been plotted in normalised units for a constant value of α ($=3$) at $n = 5$, 10 and 20.

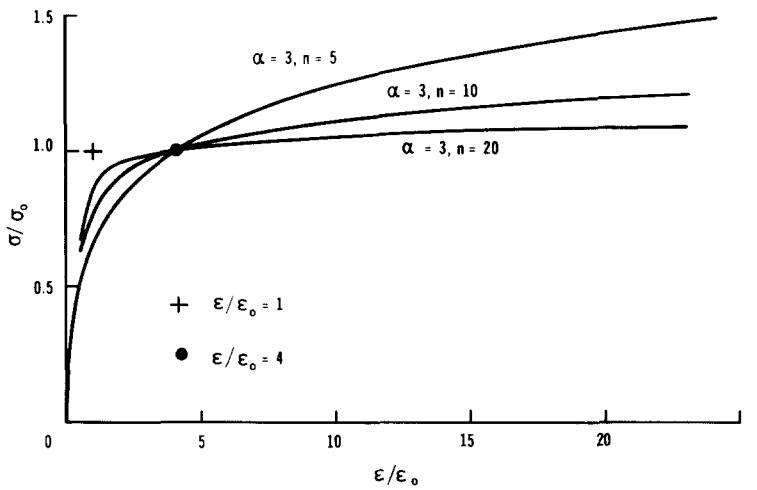

Fig. 8. Variation of stress–strain curve with n for constant α and σ_o.

It is apparent that not only is a decrease in n equivalent to an increase in the implied ultimate tensile stress, but it is also equivalent to a decrease in the implied yield stress as defined by the point where the curve first become significantly non-linear. Thus, an excessive degree of non-linearity occurs below σ_o when high values of α are coupled with low values of n.

In evaluating J, the solution is dominated by α at low stress levels and by n at high stress levels. Thus, if α is high, excessive plasticity effects will be predicted at stress levels well below net section yield, as demonstrated in Figs 2(b) and 3(b). To avoid this, a low value of α is needed, and this

clearly gives a better fit to the experimental data at low stress levels (Fig. 7). A low value of n tends to underestimate the plasticity effects at high stress levels, often to such a degree that the plastic collapse limit is either badly, or wrongly, defined (see Figs 2(a) and (b)). High values of n tend to overestimate plasticity effects. In this case the plastic collapse limit will still be wrongly defined, but it will tend to be underestimated. Thus, the J solution which used a low α and a high n for the austenitic material gave a good fit to the experimental data at stress levels close to net section yield but over-predicted plasticity effects at higher stress levels.

The properties exhibited in Fig. 8 should also be borne in mind if the Ramberg–Osgood law is used to study the effect of strain hardening capacity on J estimates. In this type of exercise it is common to fix σ_o and α and vary n (Kumar *et al.*[3]). Since this has the effect of rotating the predicted stress–strain curve about the point $\varepsilon = \varepsilon_o(1+\alpha)$, $\sigma = \sigma_o$, it also has the effect of varying the implied yield stress. This must be taken into account when comparisons are made on this basis.

THE USE OF THE STRAIN HARDENING SOLUTION

The series of assessment lines plotted in Fig. 4 have been replotted in Fig. 9 after renormalising S_r by σ_y/σ_F. This allows a direct comparison to be made between the conventional R6 assessment line, where σ_F is used to

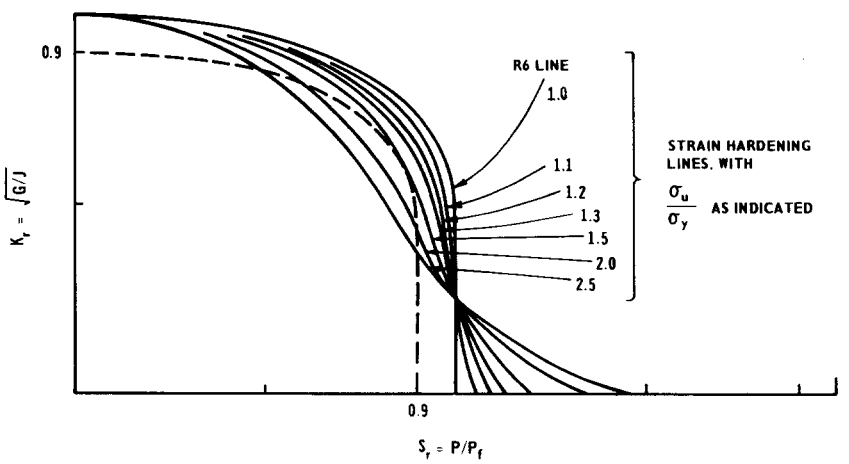

Fig. 9. Comparison of R6 assessment line with strain hardening lines of Fig. 4.

define the plastic collapse limit, and the strain hardening form for R6 proposed in eqn. (6). The two forms of solution are exactly equivalent at $S_r = 0$, $K_r = 1$ and at $S_r = 1$, $K_r = 0{\cdot}25$, where S_r is defined as P/P_F. Elsewhere, the mismatch between the strain hardening solution and the conventional solution depends upon the value of K_r and the ratio σ_u/σ_y. For example, at values of $K_r > 0{\cdot}2$ the maximum difference between the solutions is 6 per cent in terms of loads for a steel similar to A533B (where $\sigma_u/\sigma_y \simeq 1{\cdot}3$) while it is 21 per cent for an austenitic steel ($\sigma_u/\sigma_y \simeq 2{\cdot}5$). Inaccuracies of 6 per cent in load are well within the tolerance required of any analysis, but potential errors of 20 per cent must give cause for concern. The dashed line has been drawn at a position 10 per cent inside the conventional assessment line. If this is regarded as the limit beyond which potential non-conservative inaccuracies cannot be tolerated, then the flow stress criterion required of the conventional R6 procedures would be unacceptable for ratios of $\sigma_u/\sigma_y > 1{\cdot}5$. On this basis, for most structural ferritic steels the conventional R6 procedures are satisfactory.

For materials with $\sigma_u/\sigma_y > 1{\cdot}5$ and, in particular, austenitic materials, the conventional R6 procedures risk being non-conservative. In such cases Fig. 4 can be used as a strain hardening assessment diagram, following the basic principles of R6, but with S_r referred to σ_y rather than σ_F. This requires the plotting on the diagram of an assessment point[10] or an assessment locus[5,11] as required. The acceptability of this point or locus is then judged against the relevant assessment line defined by the ratio of σ_u/σ_y.

For example, in Fig. 10 a locus of assessment points, ABCDE, is plotted at an applied load, L, as a function of postulated crack growth, Δa, with:

$$S_r = \frac{L}{L_y(a + \Delta a)}$$

and:

$$K_r = \frac{K_1(L, a + \Delta a)}{\sqrt{E' J_R(\Delta a)}}$$

where $L_y(a + \Delta a)$ is the load to yield the uncracked ligament, $K_1(L, a + \Delta a)$ is the applied stress intensity factor, $J_R(\Delta a)$ is the J resistance curve and E' is the effective Young's modulus, E, for plane stress and $E/1 - \nu^2$ for plane strain, ν being Poisson's ratio. The material

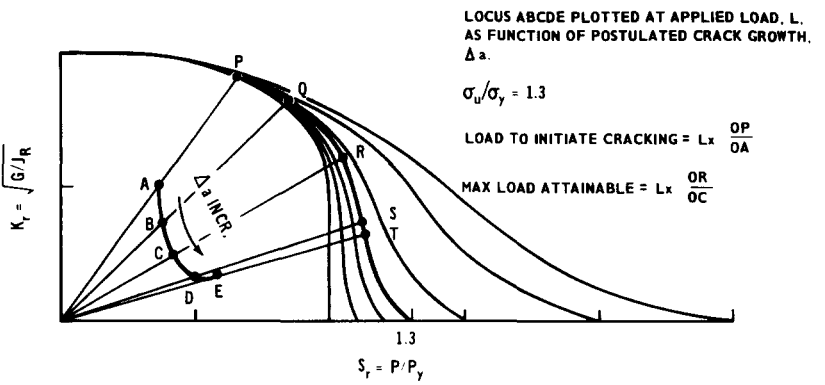

Fig. 10. Use of strain hardening assessment diagram.

is a ferritic steel, with $\sigma_u/\sigma_y = 1{\cdot}3$, so the assessment must be judged against the assessment line for $\sigma/\sigma_y = 1{\cdot}3$.

The structure is highly stable at the applied load, since all points on the locus lie well below the relevant assessment line. Reserve factors can be defined as the ratio of the load required to project a point to the assessment line to the load applied.[10] This means that the load to initiate cracking is given by:

$$L_A = \frac{OP}{OA} \times L$$

the load to extend the crack to B is given by:

$$L_B = \frac{OQ}{OB} \times L$$

The maximum load attainable is given by the product of the maximum in these reserve factors and the applied load. This occurs at C so

$$L_{max} = \frac{OR}{OC} \times L$$

There are certain advantages to this form of analysis over other procedures. First, elastic–plastic solutions can be obtained for materials for which α and n are unknown or are badly defined. This is of particular advantage when dealing with older plant, or materials which have a large scatter in their flow properties, or where material degradation is likely in service. Secondly, explicit use of the plastic yield load, and, by extension, the plastic collapse load, provides important safeguards against

overestimating the load capacity of structures. This safeguard is particularly useful when dealing with materials with a high capacity for strain hardening, where a good fit between stress–strain curves at high strains and the Ramsberg–Osgood law can only be obtained with a low value of n. Thirdly, it allows analysis procedures for secondary stresses (thermal and residual stresses) to be incorporated using the procedures developed by Milne.[12] The estimation scheme developed by Kumar *et al.*[3] cannot be applied to secondary stresses without modification. Fourthly, by separating the variables in the diagrammatic form of Fig. 10 it allows a sensitivity analysis on the input data to be performed in a very simple and straightforward fashion. This can have an important influence over the degree of coincidence obtained from an analysis and may be used to allow a relaxation in the safety factors normally required.[10]

CONCLUSIONS

(1) For structures made of ferritic steels, the conventional R6 procedures can be expected to give results comparable to J estimates.
(2) For structures made of austenitic steels an extra allowance has to be made for strain hardening.
(3) The Ramberg–Osgood law provides an unsatisfactory fit to the stress–strain curves of austenitic steels and results in erroneous estimates for J.
(4) A strain hardening form of the R6 diagram has been developed which overcomes most of those objections.

ACKNOWLEDGEMENTS

This work was done at the Central Electricity Research Laboratories and is published by permission of the Central Electricity Generating Board.

REFERENCES

1. Chell, G. G., ASTM STP 668, 1979, p. 581.
2. Bloom, J. M., *Proc. of EPRI Ductile Fracture Public Meeting, Palo Alto, California*, December, 1980.

3. Kumar, V., German, M. D. and Shih, C. F., *GE Report No. SRD-80-094* (to EPRI), 1980.
4. Milne, I., *Experimental validation of resistance curve analysis*, CERL Note No. RD/L/2044N81, 1981.
5. Chell, G. G. and Milne, I., *A simple practical method for determining the ductile instability of cracked structures*, CERL Note No. RD/L/N 87/79, published in *Proc. of CSNI Specialist Meeting on Plastic Tearing Instability at St. Louis, 1979*, NUREG/CP-0010, CSNI Report No. 39, 1979.
6. Issler, L., Birk, R. and Hund, R., *Proc. of 6MPA Seminar*, MPA, Stuttgart, 1980.
7. Newman, J. C., ASTM Task Group E24.06.02. Predictive 'Round Robin' on Fracture, 1979.
8. Kanninen, M. F., Marschall, C. W., Broek, D., Sampath, S. G., Abon Sayed, I. S, Wilkowski, G. and Zahoor, A., Battelle (Columbus) Report No. T-118-2 (to EPRI), 1980.
9. Haigh, J. R. and Richards, C. R., *Yield point loads and compliance functions of fracture mechanics specimens*, CERL Memorandum No. RD/L/M 461, 1974.
10. Milne, I., Harrison, R. P. and Dowling, A. R., *Proc. of Fourth Int. Conf. on Pressure Vessel Technology*, I. Mech. E. London. Paper C11/80, 1980.
11. Milne, I., *Failure analysis in the presence of ductile crack growth*, CERL Note No. RD/L/N 179/78. *Mats. Sci. and Eng.*, **39** (1979), p. 65.
12. Milne, I., *Assessment of the defect tolerance of structures subjected to combined secondary and primary loads*. CERL Note No. RD/L/N 112/78. In: *SMiRT 5 (Berlin) 1979*. Paper G1/3, 1978.